Supporting Information:

Vibrational Spectroscopy of Fluoroformate, FCO_2^-, Trapped in Helium Nanodroplets

*Daniel A. Thomas, Eike Mucha, Sandy Gewinner, Wieland Schöllkopf, Gerard Meijer, and Gert von Helden**

Fritz-Haber-Institut der Max-Planck-Gesellschaft, Faradayweg 4-6, 14195 Berlin, Germany

Corresponding Author

*Email: helden@fhi-berlin.mpg.de

Table of Contents

Low-Intensity Features in the Spectrum of FCO_2^-

As noted briefly in the main text, the presented infrared spectra correspond to the integrated intensity over a given *m/z* range measured on a time-of-flight mass spectrometer as a function of the incident photon energy. Each region of the spectrum is measured in triplicate to verify reproducibility. In addition to the features discussed in the main text, several weak transitions are observed with a relative intensity of < 1%. An enlargement of the spectrum is shown in Figure S1 to make these weak absorptions more visible. Most notably, additional weak but reproducible features are observed at 522, 804, 839, 1275, and 1726 cm^{-1}.

Two of these features may correspond to the weaker fundamental vibrational transitions of FCO_2^-, the C–F bending mode δ(C–F) and the out-of-plane deformation γ(FCO_2). The feature at 522 cm^{-1} is very close to the value of δ(C–F) anticipated based on the difference between the deperturbed values for the combination band δ(C–F) + $\nu_s(COO^-)$ and the fundamental $\nu_s(COO^-)$, which yields a value of 520 cm^{-1}. The experimental feature at 839 cm^{-1} may correspond to γ(FCO_2), although this frequency is ~30 cm^{-1} higher than that predicted by theory.

An additional source of low-intensity features is the pickup of background gas molecules, most notably water and molecular nitrogen, by the helium nanodroplet. Based on the background pressure of 2-5 × 10^{-9} mbar for these gases measured utilizing a residual gas analyzer, we estimate that approximately 1-3% of droplets will contain both an ion and a water or nitrogen molecule. During the ion ejection process, the ion-neutral complex may dissociate, leading to the detection of the free ion in the mass spectrum and a corresponding feature in the infrared spectrum. The association of nitrogen is expected to result in only minor shifts of the vibrational modes, but the presence of water likely yields distinct vibrational transitions. For example, the

vibrational mode at 804 cm^{-1} in Figure S1 likely results from dissociation of the FCO_2^--water complex, as a signal at *m/z* 81 is also detected in the mass spectrum at this photon energy.

The weak feature observed at 1275 cm^{-1} arises from a small amount of HCO_3^- that is also present in the hexapole ion trap. Due to the low resolution of the TOF-MS, the peak centered at *m/z* 61 also yields a small amount of signal in the integration window utilized for FCO_2^- detection (~ *m/z* 62-64.5).

The feature at 1726 cm^{-1} remains unassigned. The corresponding mass spectrum contains no clear signals at other *m/z* values, and the observed ion counts are centered at *m/z* 63.

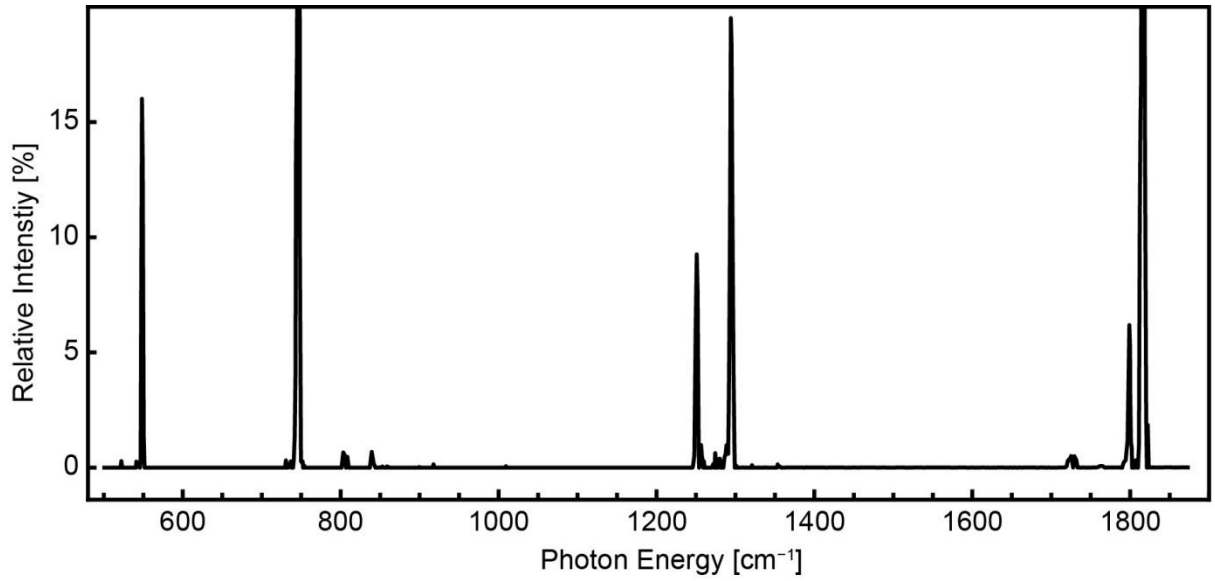

Figure S1. Magnification of experimental IR spectrum of FCO_2^- trapped in helium nanodroplets; weak but reproducible features are observed at 522, 804, 839, 1275, and 1726 cm^{-1}.

Fermi Resonance Analysis

The intensities and frequencies of the Fermi doublet can be analyzed by first-order perturbation theory for degenerate modes. Following the notation of Herzberg,[1] the two participating vibrational levels *n* and *i* have unperturbed eigenfunctions ψ_n^0 and ψ_i^0 and eigenvalues E_n^0 and E_i^0. Applying the first-order perturbation defined by the perturbation function *W* yields the matrix equation

$$\begin{pmatrix} E_n^0 & W_{ni} \\ W_{in} & E_i^0 \end{pmatrix} \begin{pmatrix} \psi_n \\ \psi_i \end{pmatrix} = E \begin{pmatrix} \psi_n \\ \psi_i \end{pmatrix} \quad \text{(S1)}$$

with eigenvalue matrix *E*, eigenfunctions ψ_n and ψ_i, and perturbative off-diagonal matrix elements

$$W_{ni} = \int \psi_n^0 \, W \psi_i^{0*} d\tau \quad \text{(S2)}$$

Solving the secular determinant equation

$$\begin{vmatrix} E_n^0 - E & W_{ni} \\ W_{in} & E_i^0 - E \end{vmatrix} = 0 \quad \text{(S3)}$$

yields the eigenvalues corresponding to the perturbed energies of the vibrational levels

$$E = \left(\frac{E_n^0 + E_i^0}{2}\right) \pm \frac{1}{2}\sqrt{4|W_{ni}|^2 + \delta^2} \quad \text{(S4)}$$

where $\delta = E_n^0 - E_i^0$ is the energy difference of the unperturbed levels. Solving for the eigenfunctions ψ_n and ψ_i yields

$$\psi_n = \beta\psi_n^0 - \sqrt{1-\beta^2}\psi_i^0 \quad \text{(S5)}$$

$$\psi_i = \sqrt{1-\beta^2}\psi_n^0 + \beta\psi_i^0 \quad \text{(S6)}$$

where

$$\beta = \left(\frac{\sqrt{4|W_{ni}|^2+\delta^2}+\delta}{2\sqrt{4|W_{ni}|^2+\delta^2}}\right)^{1/2} \quad \text{(S7)}$$

The relative intensities of the two vibrational transitions in the Fermi doublet can also be analyzed by first-order perturbation theory. For transitions with approximately the same energy, the observed intensity of a given transition is proportional to the absolute square of the expectation value of the transition dipole moment operator, $|\langle\psi_a|\hat{\mu}|\psi_b\rangle|^2$. Within the context of the Fermi resonance, we make the approximation that the transition from the ground state ψ_0 to the unperturbed state ψ_n^0 has a nonzero transition probability, whereas the transition from ψ_0 to ψ_i^0 has zero probability:

$$|\langle\psi_n^0|\hat{\mu}|\psi_0\rangle|^2 > 0 \quad \text{(S8)}$$

$$\left|\langle\psi_i^0|\hat{\mu}|\psi_0\rangle\right|^2 \cong 0 \quad \text{(S9)}$$

Since the eigenfunctions following perturbation are a linear combination of the unperturbed eigenfunctions, the intensities I_n and I_i of the two components of the Fermi doublet depend on the weighting coefficient of the linear combination (equations S5-S7):

$$I_n \sim |\langle\psi_i|\hat{\mu}|\psi_0\rangle|^2 = \beta^2|\langle\psi_n^0|\hat{\mu}|\psi_0\rangle|^2 \quad \text{(S10)}$$

$$I_i \sim |\langle\psi_i|\hat{\mu}|\psi_0\rangle|^2 = (1-\beta^2)|\langle\psi_n^0|\hat{\mu}|\psi_0\rangle|^2 \quad \text{(S11)}$$

To derive values for the interaction parameter $\alpha = (|W_{ni}|^2)^{1/2}$ (also referred to as simply W)[2] as well as the energies of the deperturbed vibrational modes, the equations here must be related to values measured experimentally. First, we designate Δ as the measured energy difference between the two features of the Fermi doublet and note that according to equation S4,

$$\Delta = \sqrt{4|W_{ni}|^2 + \delta^2} \quad \text{(S12)}$$

Note that substituting equation S12 into equation S7 yields

$$\beta = \left(\frac{\Delta+\delta}{2\Delta}\right)^{1/2} = \left(\frac{1}{2} + \frac{\delta}{2\Delta}\right)^{1/2} \quad \text{(S13)}$$

Additionally, we define *n* as the intensity ratio between the weak and strong transitions measured experimentally,

$$n = \frac{I_{strong}}{I_{weak}} = \frac{I_n}{I_i} \cong \frac{\beta^2}{1-\beta^2} = \frac{\frac{\Delta+\delta}{2\Delta}}{\frac{\Delta-\delta}{2\Delta}} = \frac{\Delta+\delta}{\Delta-\delta} \qquad \text{(S14)}$$

Solving equation S14 for the energy difference of the unperturbed modes δ, one obtains

$$\delta = \frac{(n-1)}{(n+1)}\Delta \qquad \text{(S15)}$$

and solving equation S12 for the interaction parameter α yields

$$\alpha = (|W_{ni}|^2)^{1/2} = \left(\frac{\Delta^2-\delta^2}{4}\right)^{1/2} = \frac{\sqrt{n}}{n+1}\Delta \qquad \text{(S16)}$$

Shown in Table S1 are the parameters calculated utilizing the analysis outlined above. It should be noted that the relative intensities measured experimentally result from an ion ejection process that is nonlinear with respect to transition strength. Thus, the intensity ratios may be distorted, especially for the Fermi resonance between $\nu_{as}(COO^-)$ and $\delta(C–F) + \nu_s(COO^-)$, where there is a large difference in the measured intensities.

Table S1. Fermi Resonance Parameters Derived from Experimental Frequencies and Intensities.[a]

Resonant Vibrational Levels	**Symm. Species**	**Fermi Doublet Line 1**	**Fermi Doublet Line 2**	**Doublet Spacing (Δ)**	**Intensity Ratio (*n*)**	**Deperturbed Spacing (δ)**	**Interaction Parameter (α)**
$\nu_s(COO^-)$, ν(C–F) + δ(OCO)	A_1	1251	1294	43	2.1	15	20.
$\nu_{as}(COO^-)$, δ(C–F) + $\nu_s(COO^-)$	B_2	1799	1816	17	16	15	4.

a. All values reported in wavenumbers (cm^{-1})

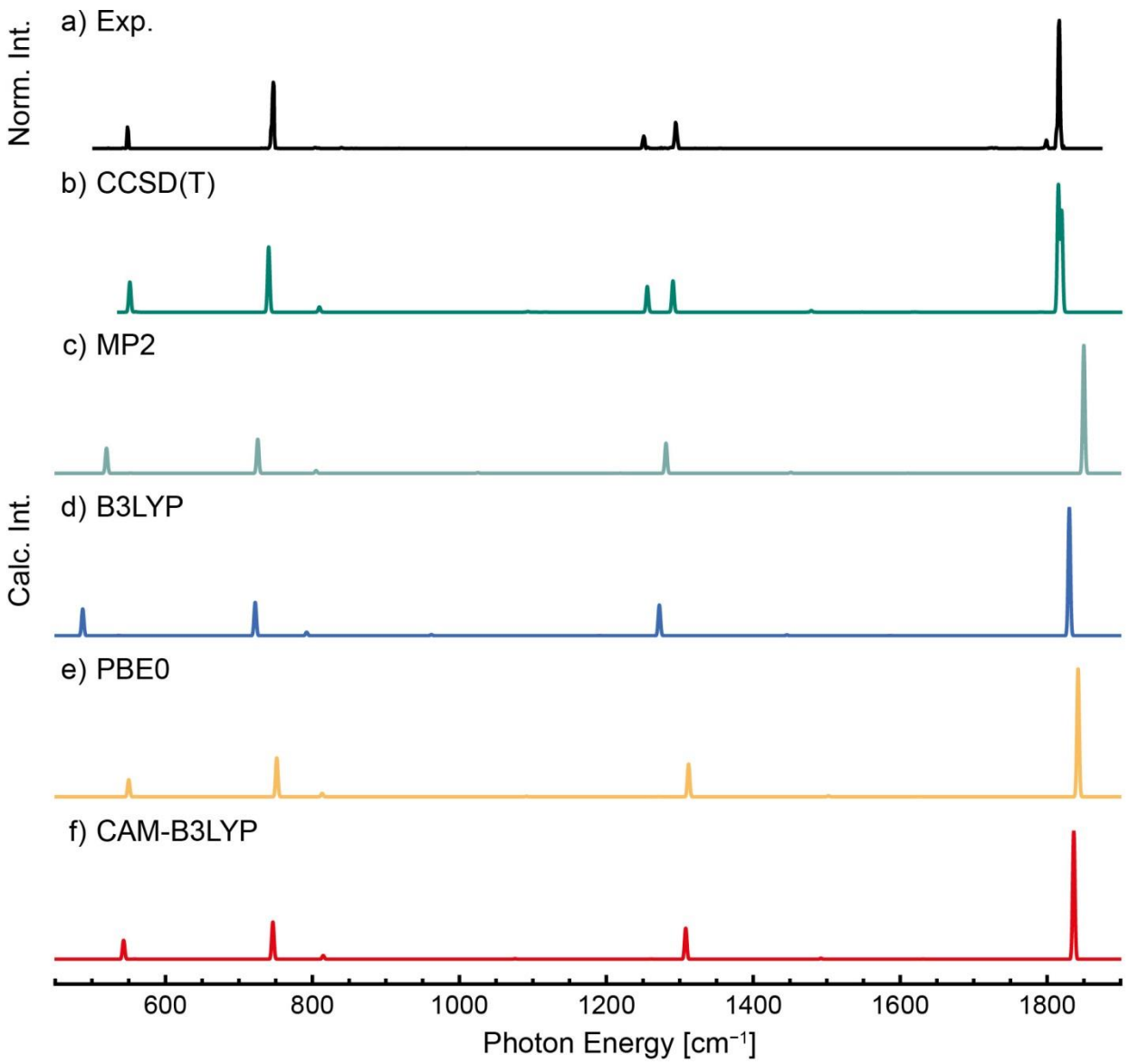

Figure S2. Vibrational spectrum of fluoroformate obtained using the helium nanodroplet method (a) compared to spectra obtained by *ab initio* calculations using the (G)VPT2 approach (b-f). CCSD(T) calculations were carried out within the CFOUR program utilizing the VPT2 approach, and all other were calculations were performed within Gaussian 09 using the GVPT2 method. MP2 calculations utilized the d-aug-cc-pVQZ basis set, and all other theoretical methods utilized the aug-cc-pVTZ basis set.

Table S2. Experimental and Theoretical Values for the Vibrational Frequencies of Fluoroformate.[a]

Vib.	Symm. Species	Exp.	CCSD(T) harm.[b,c]	MP2 harm.[d,e]	PBE0 harm.[c,d]	B3LYP harm.[c,d]	CAM-B3LYP harm.[c,d]	CCSD(T) VPT2[b,c]	MP2 GVPT2[d,e]	PBE0 GVPT2[c,d]	B3LYP GVPT2[c,d]	CAM-B3LYP GVPT2[c,d]
ν(C–F)	A_1	548	571.6	543.4	567.5	507.3	562.2	551.5	519.8	550.0	487.4	543.1
δ(C–F)	B_2	-	569.3	563.3	568.9	546.4	567.6	559.3	552.6	559.8	536.4	558.0
δ(OCO)	A_1	747	760.0	742.3	767.7	735.1	762.8	740.4	725.6	751.5	722.2	746.2
γ(FCO_2)	B_1	-	819.2	815.3	821.5	800.8	823.4	809.5	805.0	813.2	792.2	814.7
ν(C–F) + δ(OCO)	A_1	1251[f] (1265)[g]	1331.5	1285.8	1335.2	1242.5	1325.0	1290.7[f]	1219.0[f] (1229.4)[h]	1271.2[f] (1287.5)[h]	1190.6[f] (1196.8)[h]	1261.3[f] (1274.5)[h]
$\nu_s(COO^-)$	A_1	1294[f] (1280)[g]	1298.8	1295.4	1321.7	1291.5	1321.3	1255.8[f]	1281.3[f] (1270.8)[h]	1312.0[f] (1295.7)[h]	1272.2[f] (1266.0)[h]	1308.1[f] (1294.9)[h]
δ(C–F) + $\nu_s(COO^-)$	B_2	1799[f] (1800)[g]	1868.2	1858.7	1890.6	1837.9	1888.9	1819.8[f]	1818.3[f] (1821.3)[h]	1863.2[f] (1853.4)[h]	1796.9[f] (1800.7)[h]	1859.1[f] (1850.8)[h]
$\nu_{as}(COO^-)$	B_2	1816[f] (1815)[g]	1852.3	1872.7	1879.9	1855.3	1873.0	1815.3[f]	1849.9[f] (1846.9)[h]	1842.1[f] (1851.9)[h]	1830.2[f] (1826.4)[h]	1836.3[f] (1844.6)[h]

a. All values reported in wavenumbers (cm^{-1})
b. Calculations carried out using the CFOUR computational chemistry package[3]
c. The aug-cc-pVTZ basis set was utilized
d. Calculations carried out with the Gaussian 09 program[4]
e. The d-aug-cc-pVQZ basis set was utilized
f. Frequency in Fermi doublet
g. Deperturbed frequencies derived from experimental intensities and frequencies using first-order perturbation theory
h. Deperturbed frequencies obtained from GVPT2 calculations[5]

Table S3. Experimental and Theoretical Values for the Vibrational Frequencies of Formate.[a]

Vibration	Symm. Species	Exp.	Exp. Lit.	Theory Lit.[d]	CCSD(T) harm.[e,f]	MP2 harm.[f,g]	B3LYP harm.[f,g]	CCSD(T) VPT2[e,f]	MP2 VPT2[f,g]	B3LYP VPT2[f,g]
δ(OCO)	A_1	-	743[b]	738.0	744.7	737.7	744.4	738.7	732.1	738.8
γ(HCO_2)	B_2	-	-	1030.3	1055.3	1046.0	1042.7	1035.9	1024.9	1022.2
ν_s(COO^-)	A_1	1317	1314[c]	1316.4	1344.5	1332.7	1338.6	1318.4	1308.9	1312.1
δ(C–H)	B_1	-	-	1340.7	1380.7	1376.6	1370.8	1345.2	1341.4	1335.3
ν_{as}(COO^-)	B_1	1623	1622[c]	1619.1	1662.5	1648.1	1650.0	1633.0	1620.9	1621.6
ν(C–H)	A_1	-	2449[c]	2441.2	2670.6	2699.9	2568.4	2424.1	2482.2	2344.1

a. All values reported in wavenumbers (cm^{-1})
b. Values taken from reference 6
c. Values taken from reference 7
d. Values taken from reference 8
e. Calculations carried out using the CFOUR computational chemistry package
f. The aug-cc-pVTZ basis set was utilized
g. Calculations carried out with the Gaussian 09 program

Table S4. Comparison of Experimental Intensities and Frequencies of Fluoroformate to Theoretical Values at the CCSD(T)/aug-cc-pVTZ Level of Theory.

Vib.	Symm. Species	Experimental Frequency [cm^{-1}]	Experimental Relative Intensity [%]	CCSD(T)[a] Harmonic Frequency [cm^{-1}]	CCSD(T)[a] Harmonic Intensity [km/mol]	CCSD(T) VPT2[a] Frequency [cm^{-1}]	CCSD(T) VPT2[a] Intensity [km/mol]	CCSD(T) VPT2[a] Relative Intensity [%]
ν(C–F)	A_1	548	17	571.6	95.7	551.5	121.3	23.7
δ(C–F)	B_2	-		569.3	1.5	559.3	1.5	0.3
δ(OCO)	A_1	747	52	760.0	281.0	740.4	262.8	51.3
γ(FCO_2)	B_1	-		819.2	21.3	809.5	20.8	4.1
ν(C–F) + δ(OCO)	A_1	1251[b] (1265)[c]	20.	1331.5	0.0	1290.7[b]	125.9	24.6
$\nu_s(COO^-)$	A_1	1294[b] (1280)[c]	9.6	1298.8	222.9	1255.8[b]	103.5	20.2
δ(C–F) + $\nu_s(COO^-)$	B_2	1799[b] (1800)[c]	6.4	1868.2	0.0	1819.8[b]	405.3	79.2
$\nu_{as}(COO^-)$	B_2	1816[b] (1815)[c]	100	1852.3	904.8	1815.3[b]	511.8	100

a. Calculations carried out using the CFOUR computational chemistry package[3]
b. Frequency in Fermi doublet
c. Deperturbed frequencies derived from experimental intensities and frequencies using first-order perturbation theory

Table S5. Comparison of Experimental Intensities and Frequencies of Fluoroformate to Theoretical Values at the MP2/d-aug-cc-pVTZ Level of Theory.

Vib.	Symm. Species	Experimental Frequency [cm^{-1}]	Experimental Relative Intensity [%]	MP2[a] Harmonic Frequency [cm^{-1}]	MP2[a] Harmonic Intensity [km/mol]	MP2 GVPT2[a] Frequency [cm^{-1}]	MP2 GVPT2[a] Intensity [km/mol]	MP2 GVPT2[a] Relative Intensity [%]
ν(C–F)	A_1	548	17	543.4	144.6	519.8	170.4	19.5
δ(C–F)	B_2	-	-	563.3	1.7	552.6	1.7	0.2
δ(OCO)	A_1	747	52	742.3	254.1	725.6	231.6	26.6
γ(FCO_2)	B_1	-	-	815.3	18.3	805.0	17.8	2.0
ν(C–F) + δ(OCO)	A_1	1251[b] (1265)[c]	20.	1285.8	0.0	1219.0[b] (1229.4)[d]	1.3	0.1
$\nu_s(COO^-)$	A_1	1294[b] (1280)[c]	9.6	1295.4	210.9	1281.3[b] (1270.8)[d]	204.7	23.5
δ(C–F) + $\nu_s(COO^-)$	B_2	1799[b] (1800)[c]	6.4	1858.7	0.0	1818.3[b] (1821.3)[d]	0.1	0.0
$\nu_{as}(COO^-)$	B_2	1816[b] (1815)[c]	100	1872.7	901.7	1849.9[b] (1846.9)[d]	871.9	100

a. Calculations carried out with the Gaussian 09 program[4]
b. Frequency in Fermi doublet
c. Deperturbed frequencies derived from experimental intensities and frequencies using first-order perturbation theory
d. Deperturbed frequencies obtained from GVPT2 calculations[5]

Table S6. Comparison of Experimental Intensities and Frequencies of Fluoroformate to Theoretical Values at the PBE0/aug-cc-pVTZ Level of Theory.

Vib.	Symm. Species	Experimental Frequency [cm^{-1}]	Experimental Relative Intensity [%]	PBE0[a] Harmonic Frequency [cm^{-1}]	PBE0[a] Harmonic Intensity [km/mol]	PBE0 GVPT2[a] Frequency [cm^{-1}]	PBE0 GVPT2[a] Intensity [km/mol]	PBE0 GVPT2[a] Relative Intensity [%]
ν(C–F)	A_1	548	17	567.5	95.0	550.0	113.7	13.3
δ(C–F)	B_2	-	-	568.9	1.6	559.8	1.5	0.2
δ(OCO)	A_1	747	52	767.7	275.3	751.5	259.1	30.4
γ(FCO_2)	B_1	-	-	821.5	22.8	813.2	22.7	2.7
ν(C–F) + δ(OCO)	A_1	1251[b] (1265)[c]	20.	1335.2	0.0	1271.2[b] (1287.5)[d]	1.3	0.1
$\nu_s(COO^-)$	A_1	1294[b] (1280)[c]	9.6	1321.7	224.7	1312.0[b] (1295.7)[d]	217.5	25.5
δ(C–F) + $\nu_s(COO^-)$	B_2	1799[b] (1800)[c]	6.4	1890.6	0.0	1863.2[b] (1853.4)[d]	0.1	0.0
$\nu_{as}(COO^-)$	B_2	1816[b] (1815)[c]	100	1879.9	891.1	1842.1[b] (1851.9)[d]	852.8	100

a. Calculations carried out with the Gaussian 09 program[4]
b. Frequency in Fermi doublet
c. Deperturbed frequencies derived from experimental intensities and frequencies using first-order perturbation theory
d. Deperturbed frequencies obtained from GVPT2 calculations[5]

Table S7. Comparison of Experimental Intensities and Frequencies of Fluoroformate to Theoretical Values at the B3LYP/aug-cc-pVTZ Level of Theory.

Vib.	Symm. Species	Experimental Frequency [cm^{-1}]	Experimental Relative Intensity [%]	B3LYP[a] Harmonic Frequency [cm^{-1}]	B3LYP[a] Harmonic Intensity [km/mol]	B3LYP GVPT2[a] Frequency [cm^{-1}]	B3LYP GVPT2[a] Intensity [km/mol]	B3LYP GVPT2[a] Relative Intensity [%]
ν(C–F)	A_1	548	17	507.3	162.7	487.4	176.8	20.8
δ(C–F)	B_2	-	-	546.4	1.5	536.4	1.5	0.2
δ(OCO)	A_1	747	52	735.1	238.6	722.2	220.7	26.0
γ(FCO_2)	B_1	-	-	800.8	23.1	792.2	23.1	2.7
ν(C–F) + δ(OCO)	A_1	1251[b] (1265)[c]	20.	1242.5	0.0	1190.6[b] (1196.8)[d]	1.1	0.1
$\nu_s(COO^-)$	A_1	1294[b] (1280)[c]	9.6	1291.5	209.9	1272.2[b] (1266.0)[d]	202.8	23.9
δ(C–F) + $\nu_s(COO^-)$	B_2	1799[b] (1800)[c]	6.4	1837.9	0.0	1796.9[b] (1800.7)[d]	0.1	0.1
$\nu_{as}(COO^-)$	B_2	1816[b] (1815)[c]	100	1855.3	884.4	1830.2[b] (1826.4)[d]	848.0	100

a. Calculations carried out with the Gaussian 09 program[4]
b. Frequency in Fermi doublet
c. Deperturbed frequencies derived from experimental intensities and frequencies using first-order perturbation theory
d. Deperturbed frequencies obtained from GVPT2 calculations[5]

Table S8. Comparison of Experimental Intensities and Frequencies of Fluoroformate to Theoretical Values at the CAM-B3LYP/aug-cc-pVTZ Level of Theory.

Vib.	Symm. Species	Experimental Frequency [cm^{-1}]	Experimental Relative Intensity [%]	CAM-B3LYP[a] Harmonic Frequency [cm^{-1}]	CAM-B3LYP[a] Harmonic Intensity [km/mol]	CAM-B3LYP GVPT2[a] Frequency [cm^{-1}]	CAM-B3LYP GVPT2[a] Intensity [km/mol]	CAM-B3LYP GVPT2[a] Relative Intensity [%]
ν(C–F)	A_1	548	17	562.2	111.5	543.1	133.0	14.8
δ(C–F)	B_2	-	-	567.6	1.5	558.0	1.5	0.2
δ(OCO)	A_1	747	52	762.8	280.8	746.2	261.7	29.1
γ(FCO_2)	B_1	-	-	823.4	26.5	814.7	25.9	2.9
ν(C–F) + δ(OCO)	A_1	1251[b] (1265)[c]	20.	1325.0	0.0	1261.3[b] (1274.5)[d]	1.3	0.1
$\nu_s(COO^-)$	A_1	1294[b] (1280)[c]	9.6	1321.3	226.0	1308.1[b] (1294.9)[d]	217.5	24.2
δ(C–F) + $\nu_s(COO^-)$	B_2	1799[b] (1800)[c]	6.4	1888.9	0.0	1859.1[b] (1850.8)[d]	0.1	0.0
$\nu_{as}(COO^-)$	B_2	1816[b] (1815)[c]	100	1873.0	940.3	1836.3[b] (1844.6)[d]	900.2	100

a. Calculations carried out with the Gaussian 09 program[4]
b. Frequency in Fermi doublet
c. Deperturbed frequencies derived from experimental intensities and frequencies using first-order perturbation theory
d. Deperturbed frequencies obtained from GVPT2 calculations[5]

Table S9. Comparison of Experimental Intensities and Frequencies of Formate to Theoretical Values at the CCSD(T)/aug-cc-pVTZ Level of Theory.

Vibration	Symm. Species	Experimental Frequency [cm^{-1}]	Experimental Relative Intensity [%]	CCSD(T)[a] Harmonic Frequency [cm^{-1}]	CCSD(T)[a] Harmonic Intensity [km/mol]	CCSD(T) VPT2[a] Frequency [cm^{-1}]	CCSD(T) VPT2[a] Intensity [km/mol]	CCSD(T) VPT2[a] Relative Intensity [%]
δ(OCO)	A_1	-	-	744.7	18.8	738.7	20.7	2.5
γ(HCO_2)	B_2	-	-	1055.3	0.2	1035.9	0.5	0.1
ν_s(COO^-)	A_1	1317	4.5	1344.5	107.7	1318.4	123.2	14.7
δ(C–H)	B_1	-	-	1380.7	10.6	1345.2	8.0	0.9
ν_{as}(COO^-)	B_1	1623	100	1662.5	866.8	1633.0	837.7	100
ν(C–H)	A_1	-	-	2670.6	477.4	2424.1	136.9	16.3

a. Calculations carried out using the CFOUR computational chemistry package[3]

Table S10. Comparison of Experimental Intensities and Frequencies of Formate to Theoretical Values at the MP2/aug-cc-pVTZ Level of Theory.

Vibration	Symm. Species	Experimental Frequency [cm^{-1}]	Experimental Relative Intensity [%]	MP2[a] Harmonic Frequency [cm^{-1}]	MP2[a] Harmonic Intensity [km/mol]	MP2 GVPT2[a] Frequency [cm^{-1}]	MP2 GVPT2[a] Intensity [km/mol]	MP2 GVPT2[a] Relative Intensity [%]
δ(OCO)	A_1	-	-	737.7	17.4	732.1	19.4	2.3
γ(HCO_2)	B_2	-	-	1046.0	0.0	1024.9	0.0	0.0
ν_s(COO^-)	A_1	1317	4.5	1332.7	96.7	1308.9	111.7	13.0
δ(C–H)	B_1	-	-	1376.6	5.0	1341.4	3.0	0.3
ν_{as}(COO^-)	B_1	1623	100	1648.1	880.2	1620.9	857.9	100
ν(C–H)	A_1	-	-	2699.9	482.0	2482.2	524.3	61.1

a. Calculations carried out with the Gaussian 09 program[4]

Table S11. Comparison of Experimental Intensities and Frequencies of Formate to Theoretical Values at the B3LYP/aug-cc-pVTZ Level of Theory.

Vibration	Symm. Species	Experimental Frequency [cm^{-1}]	Experimental Relative Intensity [%]	B3LYP[a] Harmonic Frequency [cm^{-1}]	B3LYP[a] Harmonic Intensity [km/mol]	B3LYP GVPT2[a] Frequency [cm^{-1}]	B3LYP GVPT2[a] Intensity [km/mol]	B3LYP GVPT2[a] Relative Intensity [%]
δ(OCO)	A_1	-	-	744.4	20.8	738.8	23.7	2.8
γ(HCO_2)	B_2	-	-	1042.7	1.1	1022.2	1.8	0.2
ν_s(COO^-)	A_1	1317	4.5	1338.6	140.4	1312.1	161.9	19.5
δ(C–H)	B_1	-	-	1370.8	10.6	1335.3	7.6	0.9
ν_{as}(COO^-)	B_1	1623	100	1650.0	858.6	1621.6	831.3	100
ν(C–H)	A_1	-	-	2568.4	593.1	2344.1	580.2	69.8

a. Calculations carried out with the Gaussian 09 program[4]

Table S12. Structural Parameters for Fluoroformate from *ab initio* Calculations.[a]

Structural Parameter	CCSD(T)[b,c]	MP2[d,e]	PBE0[c,d]	B3LYP[c,d]	CAM-B3LYP[c,d]
b(C,F)[a]	1.463	1.476	1.466	1.503	1.471
b(C,O)[a]	1.223	1.222	1.220	1.221	1.218
∠(O,C,O)[a]	136.74	137.04	136.56	137.50	136.77

a. Bond lengths are reported in Angstroms (Å), and bond angles are reported in degrees.
b. Calculations carried out using the CFOUR computational chemistry package[3]
c. The aug-cc-pVTZ basis set was utilized
d. Calculations carried out within the Gaussian 09 program[4]
e. The d-aug-cc-pVQZ basis set was utilized

Table S13. Structural Parameters for Formate from *ab initio* Calculations.[a]

Structural Parameter	CCSD(T)[b,c]	MP2[d,e]	B3LYP[c,d]
b(C, H)[a]	1.124	1.126	1.136
b(C, O)[a]	1.253	1.258	1.251
∠(O, C, O)[a]	130.37	130.16	130.37

a. Bond lengths are reported in Angstroms (Å), and bond angles are reported in degrees.
b. Calculations carried out using the CFOUR computational chemistry package[3]
c. The aug-cc-pVTZ basis set was utilized
d. Calculations carried out within the Gaussian 09 program[4]
e. The d-aug-cc-pVQZ basis set was utilized

Table S14. Partial Atomic Charges Derived from *ab initio* Calculations.

Atom	Mulliken Charge[c] CCSD(T)/ aug-cc-pVTZ[b]	ESP-Derived Charge[a] CCSD(T)/ aug-cc-pVTZ[b]	Mulliken Charge[d] MP2/ d-aug-cc-pVTZ[f]	APT Charge[e] MP2/ d-aug-cc-pVTZ[f]	Mulliken Charge[d] PBE0/ aug-cc-pVTZ[f]	APT Charge[e] PBE0/ aug-cc-pVTZ[f]
F	−0.341	−0.702	−0.953	−0.796	−0.411	−0.772
C	0.588	2.065	1.652	1.703	0.508	1.705
O	−0.512	−1.185	−0.849	−0.953	−0.549	−0.966
O	−0.512	−1.178	−0.849	−0.953	−0.549	−0.966

a. Derived from fitting of the ElectroStatic Potential (ESP) on a series of Connolly surfaces[9] with electron isodensity values of 10^{-3}, 10^{-4}, and 10^{-5} e^{-}/a_0^3 as implemented in MOLDEN[10]
b. Calculations carried out using the CFOUR computational chemistry package[3]
c. Calculated utilizing MOLDEN[10]
d. Values determined within the Gaussian 09 program[4]
e. Values determined within the Gaussian 09 program[4] from the atomic polar tensors (APT)[11]
f. Calculations carried out within the Gaussian 09 program[4]

REFERENCES

(1) Herzberg, G. *Molecular Spectra and Molecular Structure II. Infrared and Raman Spectra of Polyatomic Molecules*. D. Van Nostrand: New York, 1945.

(2) Monecke, J. Theory of Fermi Resonances in Raman and Infrared Spectra. *J. Raman Spectrosc.* **1987,** *18*, 477-479.

(3) CFOUR, Coupled-Cluster techniques for Computational Chemistry, a quantum-chemical program package by J.F. Stanton, J. Gauss, L. Cheng, M.E. Harding, D.A. Matthews, P.G. Szalay, with contributions from A.A. Auer, R.J. Bartlett, U. Benedikt, C. Berger, D.E. Bernholdt, Y.J. Bomble, O. Christiansen, F. Engel, R. Faber, M. Heckert, O. Heun, M. Hilgenberg, C. Huber, T.-C. Jagau, D. Jonsson, J. Jusélius, T. Kirsch, K. Klein, W.J. Lauderdale, F. Lipparini, T. Metzroth, L.A. Mück, D.P. O'Neill, D.R. Price, E. Prochnow, C. Puzzarini, K. Ruud, F. Schiffmann, W. Schwalbach, C. Simmons, S. Stopkowicz, A. Tajti, J. Vázquez, F. Wang, J.D. Watts and the integral packages MOLECULE (J. Almlöf and P.R. Taylor), PROPS (P.R. Taylor), ABACUS (T. Helgaker, H.J. Aa. Jensen, P. Jørgensen, and J. Olsen), and ECP routines by A. V. Mitin and C. van Wüllen. For the current version, see http://www.cfour.de.

(4) Gaussian 09, Revision D.01, M. J. Frisch, G. W. Trucks, H. B. Schlegel, G. E. Scuseria, M. A. Robb, J. R. Cheeseman, G. Scalmani, V. Barone, G. A. Petersson, H. Nakatsuji, X. Li, M. Caricato, A. Marenich, J. Bloino, B. G. Janesko, R. Gomperts, B. Mennucci, H. P. Hratchian, J. V. Ortiz, A. F. Izmaylov, J. L. Sonnenberg, D. Williams-Young, F. Ding, F. Lipparini, F. Egidi, J. Goings, B. Peng, A. Petrone, T. Henderson, D. Ranasinghe, V. G. Zakrzewski, J. Gao, N. Rega, G. Zheng, W. Liang, M. Hada, M. Ehara, K. Toyota, R. Fukuda, J. Hasegawa, M. Ishida, T. Nakajima, Y. Honda, O. Kitao, H. Nakai, T. Vreven, K. Throssell, J. A. Montgomery, Jr., J. E. Peralta, F. Ogliaro, M. Bearpark, J. J. Heyd, E. Brothers, K. N. Kudin, V. N. Staroverov, T. Keith, R. Kobayashi, J. Normand, K. Raghavachari, A. Rendell, J. C. Burant, S. S. Iyengar, J. Tomasi, M. Cossi, J. M. Millam, M. Klene, C. Adamo, R. Cammi, J. W. Ochterski, R. L. Martin, K. Morokuma, O. Farkas, J. B. Foresman, and D. J. Fox, Gaussian, Inc., Wallingford CT, 2009.

(5) Barone, V. Anharmonic Vibrational Properties by a Fully Automated Second-Order Perturbative Approach. *J. Chem. Phys.* **2005,** *122*, 014108.

(6) Garand, E.; Klein, K.; Stanton, J. F.; Zhou, J.; Yacovitch, T. I.; Neumark, D. M. Vibronic Structure of the Formyloxyl Radical (HCO_2) via Slow Photoelectron Velocity-Map Imaging Spectroscopy and Model Hamiltonian Calculations. *J. Phys. Chem. A* **2010,** *114*, 1374-1383.

(7) Gerardi, H. K.; DeBlase, A. F.; Su, X.; Jordan, K. D.; McCoy, A. B.; Johnson, M. A. Unraveling the Anomalous Solvatochromic Response of the Formate Ion Vibrational Spectrum: An Infrared, Ar-Tagging Study of the HCO_2^-, DCO_2^-, and $HCO_2^-\cdot H_2O$ Ions. *J. Phys. Chem. Lett.* **2011,** *2*, 2437-2441.

(8) Krekeler, C.; Mladenovic, M.; Botschwina, P. A Theoretical Investigation of the Vibrational States of HCO_2^- and its Isotopomers. *Phys. Chem. Chem. Phys.* **2005,** *7*, 882-887.

(9) Besler, B. H.; Merz, K. M.; Kollman, P. A. Atomic Charges Derived from Semiempirical Methods. *J. Comp. Chem.* **1990,** *11*, 431-439.

(10) Schaftenaar, G.; Noordik, J. H. Molden: a Pre- and Post-processing Program for Molecular and Electronic Structures. *J. Comput.-Aided Mol. Des.* **2000,** *14*, 123-134.

(11) Cioslowski, J. A new population analysis based on atomic polar tensors. *J. Am. Chem. Soc.* **1989,** *111*, 8333-8336.